To Appear in the Astrophysical Journal Letters
Preprint typeset using LaTeX style emulateapj v. 6/22/04

DEFINITIVE IDENTIFICATION OF THE TRANSITION BETWEEN SMALL- TO LARGE-SCALE CLUSTERING FOR LYMAN BREAK GALAXIES[1]

Masami Ouchi [2,3], Takashi Hamana [4], Kazuhiro Shimasaku [5], Toru Yamada [4], Masayuki Akiyama [6], Nobunari Kashikawa [4], Makiko Yoshida [5], Kentaro Aoki [6], Masanori Iye [4], Tomoki Saito [5], Toshiyuki Sasaki [6], Chris Simpson [7], and Michitoshi Yoshida [8]

To Appear in the Astrophysical Journal Letters

ABSTRACT

We report angular correlation function (ACF) of Lyman Break Galaxies (LBGs) with unprecedented statistical quality on the basis of 16,920 LBGs at $z = 4$ detected in the 1 deg^2 sky of the Subaru/XMM-Newton Deep Field. The ACF significantly departs from a power law, and shows an excess on small scale. Particularly, the ACF of LBGs with $i' < 27.5$ have a clear break between the small and large-scale regimes at the angular separation of $\simeq 7''$ whose projected length corresponds to the virial radius of dark halos with a mass of $10^{11-12} M_\odot$, indicating multiple LBGs residing in a single dark halo. Both on small ($2'' < \theta < 3''$) and large ($40'' < \theta < 400''$) scales, clustering amplitudes monotonically increase with luminosity for the magnitude range of $i' = 24.5 - 27.5$, and the small-scale clustering shows a stronger luminosity dependence than the large-scale clustering. The small-scale bias reaches $b \simeq 10 - 50$, and the outskirts of small-scale excess extend to a larger angular separation for brighter LBGs. The ACF and number density of LBGs can be explained by the cold dark matter model.

Subject headings: large-scale structure of universe — galaxies: formation — galaxies: high-redshift

1. INTRODUCTION

Recent observational studies have been found strong clustering in two-point angular correlation function (ACF) of Lyman break galaxies (LBGs) at $z = 3-5$, (e.g. Giavalisco & Dickinson 2001; Ouchi et al. 2001; Foucaud et al. 2003; Adelberger et al. 2003; Ouchi et al. 2004b; Hildebrandt et al. 2004; Allen et al. 2005), red galaxies at $z = 3$ (Daddi et al. 2003), and Lyα emitters (LAEs; Ouchi et al. 2003; Shimasaku et al. 2004) at $z = 5$. Even at $z = 6$, there is a piece of evidence for filamentary large (100 Mpc)-scale structures of LAEs (Ouchi et al. 2005). The distribution of high-z galaxies is fairly inhomogeneous and highly biased against matter distribution predicted by the cold dark matter (CDM) model. The estimated bias is $b \simeq 2-8$, depending on luminosity/type and redshift of galaxies. However, the shape of the ACF for high-z galaxies is not well constrained. Ouchi et al. (2001) report a 3σ excess of the ACF at $\theta < 5''$ for $z \sim 4$ LBGs, while Porciani & Giavalisco (2002) found a possible deficit of the ACF at $10'' \lesssim \theta \lesssim 30''$ for bright LBGs which they interpret as the halo exclusion effect on hosting halos with a mass of $10^{12} M_\odot$.

In the local universe, the correlation function shows a departure from a power law (e.g. Hawkins et al. 2003; Zehavi et al. 2004). The departure is reproduced in the framework of the halo occupation distribution (HOD) and the related halo models in the CDM cosmology (van den Bosch et al. 2003; Magliocchetti & Porciani 2003; Zehavi et al. 2004; Benson et al. 2001; Berlind et al. 2003), and is explained by two sources contributing to the correlation function; one for galaxy pairs residing in the same halo (1-halo term) and the other for galaxies hosted by different halos (2-halo term; see, e.g., Zehavi et al. 2004). The HOD has been also applied to clustering of galaxies at high-z (Bullock et al. 2002; Moustakas & Somerville 2002; Hamana et al. 2004). However, parameters of the models have not been constrained with similar accuracy as at low-z because of the small sample ($100-2000$ galaxies) and surveyed area ($0.01 - 0.1$deg^2).

In this paper, we present ACF of $z = 4$ LBGs with unprecedented statistical quality, on the basis of 16,920 LBGs obtained in the 1 deg^2 sky of Subaru/XMM-Newton Deep Field (SXDF; Sekiguchi et al. 2004). Throughout this paper, magnitudes are in the AB system, and we adopt $H_0 = 70 h_{70}$km s^{-1} Mpc^{-1} and $[\Omega_m, \Omega_\Lambda, n, \sigma_8] = [0.3, 0.7, 1.0, 0.9]$. To facilitate comparison with previous results, we express r_0 using h_{100}, the Hubble constant in units of 100 km s^{-1} Mpc^{-1}.

2. DATA AND SAMPLE

We carried out deep optical broad-band imaging with Subaru/Suprime-Cam in the 1 deg^2 sky of the SXDF. Our broad-band images reach $B \simeq 28.3$, $V \simeq 27.3$, $R \simeq 27.6$, $i' \simeq 27.5$, and $z' \simeq 26.5$ with a $2''$-diameter circular aperture at the 3σ level (Furusawa et al. in preparation). Typical seeing sizes (FWHM) of these images are $0''.8$. We use the i'-band selected source catalog of the SXDS $Ver1.0$ produced with SExtractor (Bertin & Arnouts 1996), which is composed of 0.7 million objects with $i' < 27.5$. We select LBGs at $z = 4.0 \pm 0.5$ on the basis of the color criteria of Ouchi et al. (2004a), i.e., $B - R > 1.2$, $R - i' < 0.7$, and $B - R > 1.6(R - i') + 1.9$,

[1] Based on data collected at Subaru Telescope, which is operated by the National Astronomical Observatory of Japan.
[2] Space Telescope Science Institute, 3700 San Martin Drive, Baltimore, MD 21218, USA; ouchi@stsci.edu.
[3] Hubble Fellow
[4] National Astronomical Observatory, Tokyo 181-8588, Japan
[5] Department of Astronomy, School of Science, University of Tokyo, Tokyo 113-0033, Japan
[6] Subaru Telescope, National Astronomical Observatory, 650 N.A'ohoku Place, Hilo, HI 96720, USA
[7] Department of Physics, University of Durham, South Road, Durham DH1 3LE, UK
[8] Okayama Astrophysical Observatory, National Astronomical Observatory, Kamogata, Okayama 719-0232, Japan

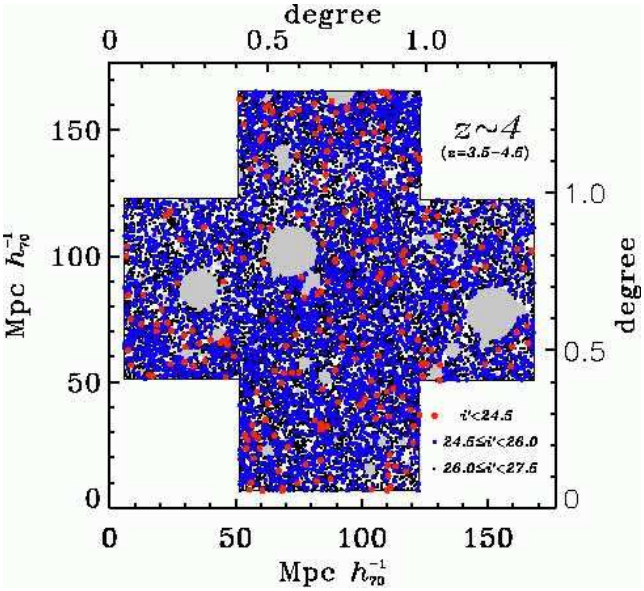

FIG. 1.— The distribution of LBGs at $z = 4.0 \pm 0.5$ in the SXDF. The red, blue, and black points denote the positions of the LBGs with $i' < 24.5$ (bright), $24.5 \leq i' < 26.0$ (intermediate), and $26.0 \leq i' < 27.5$ (faint), respectively. The gray areas present masked regions where we did not use for our analysis. The scale on the map is marked in both degrees and (comoving) megaparsecs for projected distance at $z = 4.0$. **This figure is degraded. This paper with the original figure can be downloaded from** *http : //www − int.stsci.edu/ ∼ ouchi/work/astroph/sxds_z4LBG/ouchi_highres.pdf*

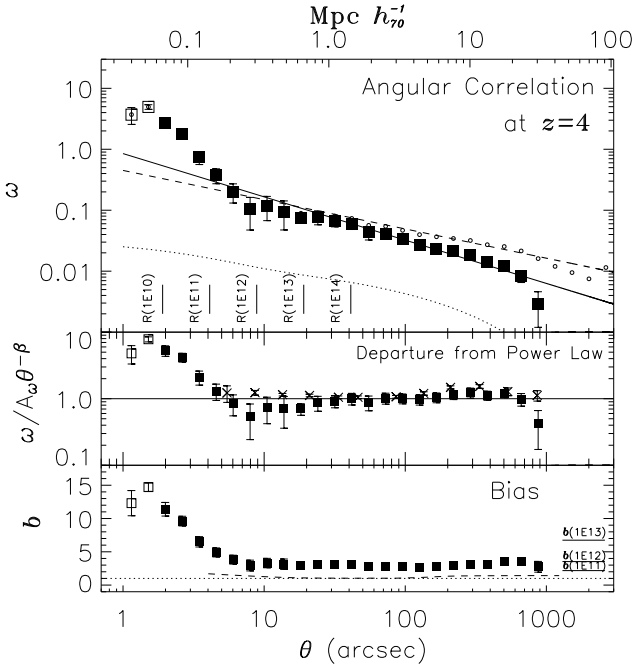

FIG. 2.— *Top* : The ACF, $\omega(\theta)$, of LBGs. The filled and open squares indicate the ACF with 1 σ bootstrap errors, while the open squares mean for ACF on very small scale which may include additional errors in source deblending and confusion. The solid line is the best-fit power law ($A_\omega\theta^{-\beta}$) for $2'' - 1000''$. The open circles are the ACF with IC correction under the assumption of the conventional power-law approximation, and the dashed lines are the best-fit power law for these open circles. The dotted curve is the ACF of dark matter predicted by the non-linear model of Peacock & Dodds (1996). The scale on the top axis denotes the projected distance in comoving megaparsecs at $z = 4.0$. The ticks labeled with R(1E10), R(1E11), R(1E12), R(1E13), and R(1E14) correspond to the predicted virial radii of dark halos, r_{200}, with a mass of 1×10^{10}, 10^{11}, 10^{12}, 10^{13}, and 10^{14} $h_{70}^{-1} M_\odot$, respectively. *Middle* : The ratios of the ACF to the best-fit power law for our LBGs (squares), together with those for local galaxies (crosses; Zehavi et al. 2004). *Bottom* : The galaxy-dark matter bias, b, of LBGs as a function of separation. The dashed curve presents bias of local galaxies (Zehavi et al. 2004). The ticks with b(1E11), b(1E12), and b(1E13) show linear biases of dark halos with a mass of 1×10^{11}, 10^{12}, and 10^{13} $h_{70}^{-1} M_\odot$, respectively, predicted by the CDM model of Sheth & Tormen (1999).

which were determined with the results of spectroscopy and Monte-Carlo simulations. We visually inspect all the candidates and mask areas contaminated with halos of bright stars and CCD blooming. Our final catalog includes 16,920 LBGs in a 1.00 deg^2 area (Table 1). Figure 1 shows the sky distribution of our LBGs. Our spectroscopic follow-up observations show that 60 out of 63 identified candidates are real LBGs at $z = 3.5 - 4.5$; i.e., 17 out of 17 and 43 out of 46 are LBGs in the SXDF (Akiyama M. in preparation) and in the Subaru Deep Field, respectively, where the latter LBG sample is made with the same color criteria as ours (Yoshida 2005). Thus, the contamination rate of our LBG sample is estimated to be $(63 - 60)/63 = 5\%$.

3. RESULTS AND DISCUSSION

3.1. *Definitive Identification of Clustering Transition*

We derive the ACF, $\omega(\theta)$, by the formula of Landy & Szalay (1993) with random samples composed of 200,000 sources, and estimate bootstrap errors (Ling et al. 1986). Since clustering properties of our 5% contaminants are not clear, we do not apply a correction for contaminants with the assumption of random distribution (c.f. Ouchi et al. 2004b). However, this correction changes $\omega(\theta)$ and bias only by 10% or less. Figure 2 presents the ACF of LBGs (top panel), residuals of a power-law fit (middle panel), and galaxy-dark matter bias (bottom panel) defined as $b(\theta) \equiv \sqrt{\omega(\theta)/\omega_{\rm dm}(\theta)}$, where $\omega_{\rm dm}(\theta)$ is the ACF predicted by the non-linear model of Peacock & Dodds (1996). In the top and middle panels of Figure 2 the ACF of LBGs shows a significant excess on small scale, and indicates that a power law, $A_\omega\theta^{-\beta}$, does not fit the data. This is the definitive identification of the departure from a power law for the ACF of LBGs at $z = 4$. With a visual inspection, we confirm that all close-pairs of LBGs are not false detections. We also plot histogram of galaxy sizes for LBG pairs. We find that most of our LBGs have FWHM$\simeq 1''$ for pairs with any separations down to, at least, $\simeq 2''$, and that extended LBGs do not boost small-scale ACF by producing false pairs. Uncertainties in source deblending and photometry can hardly account for the small-scale excess at $\gtrsim 2''$. In fact, a similar small-scale excess of ACF for $z = 4 - 5$ LBGs is also found by a recent study on high-resolution ($\sim 0''.1$) HST images (Lee et al. 2005).

Comparing our ACF with the one of dark matter, we find that the small-scale excess extends up to $\simeq 7''$, i.e. $0.24 h_{70}^{-1}$ Mpc, which is comparable to virial radius, r_{200}, of dark halos with a mass of $10^{11-12} M_\odot$ (see the ticks in the top panel of Figure 2), where r_{200} is a sphere of radius within which the mean enclosed density is 200 times the

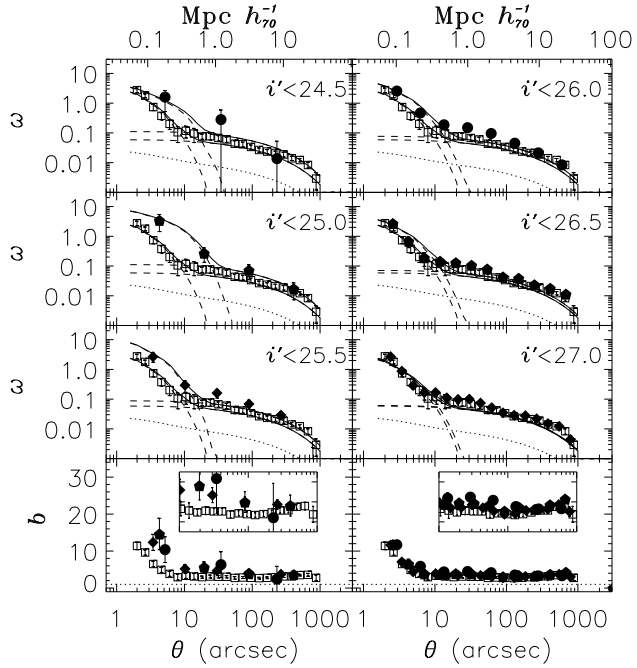

FIG. 3.— The ACFs of magnitude-limited subsamples of LBGs at $z = 4.0$. In the top to third-top panels, the filled symbols are the ACFs of our LBGs with the limiting magnitude indicated in the legend. Each of these panels shows the ACF of $i' < 27.5$ LBGs with open squares. The dotted curves are the ACF of dark matter predicted by the non-linear model of Peacock & Dodds (1996). The thick solid and dashed lines indicate the best-fit ACFs of the halo model and the breakdown of 1-halo and 2-halo terms for each subsample, while the thin lines are for $i' < 27.5$ LBGs. In the bottom panels, biases of LBGs for the each magnitude-limited subsample are presented with the symbols which correspond to those marks found in the top to third-top panels. The plots of large-scale biases are magnified in the inserted boxes.

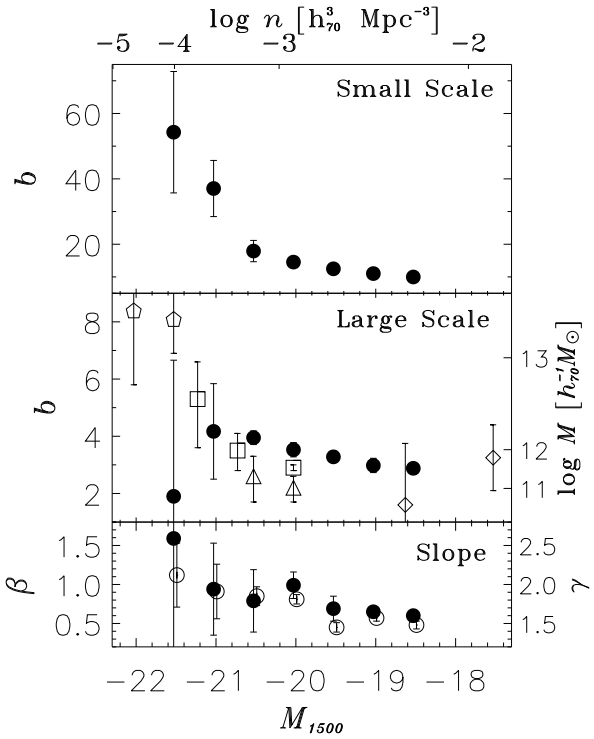

FIG. 4.— Bias and slope of $z = 4$ LBGs as a function of limiting-absolute magnitude calculated from $i' - M_{1500} = 46.0$. Top and middle panels present bias of small-scale ($2'' < \theta < 3''$) and large-scale ($40'' < \theta < 400''$) clustering. Filled circles plot for our LBGs, whose bias is directly measured from the ACFs. Open pentagons, squares, triangles, and diamonds present the large-scale ($\simeq 8h_{100}^{-1}$) bias estimated from the conventional power-law fit by Allen et al. (2005); Ouchi et al. (2004b, 2001); Arnouts et al. (2002). In the middle panel, the right-hand vertical scale means mass of dark halos corresponding to the linear bias (Sheth & Tormen 1999). The upper abscissa axis ticks number densities of our LBGs. Bottom panel shows the slope of a power law for the ACFs. Filled and open circles indicate the slopes for large-scale ($40'' < \theta < 400''$) with no IC correction ($\beta_{\rm L}$), and for all scales ($2'' < \theta < 1000''$) with IC correction (β; see Table 1), respectively.

mean cosmic value (Mo & White 2002). Interestingly, the large-scale average bias at $40'' < \theta < 400''$ is estimated to be 2.9 ± 0.2 which is also comparable to linear bias of dark halos with a mass of $10^{11-12}M_\odot$ ($b = 2.2-3.5$) predicted by the CDM (Sheth & Tormen 1999; see the ticks in the bottom panel of Figure 2). This coincidence of the dark-halo mass strongly supports that typical $z = 4$ LBGs reside in dark halos with a mass of $10^{11-12}M_\odot$. Moreover, these pieces of evidence suggest that multiple LBGs occupy a single dark halo. The middle panel of Figure 2 also plots residuals of a power-law fit for local galaxies (Zehavi et al. 2004), which is comparable to those of $z = 4$ LBGs on large scale, but significantly larger than LBGs on intermediate scale ($0.2-1.0$ Mpc) corresponding to the radius of $10^{12-14}M_\odot$ dark halos. According to the halo mass function (Sheth & Tormen 1999), the ratio of galaxy-sized halos ($10^{10-12}M_\odot$) to group/cluster-sized halos ($10^{12-14}M_\odot$) is about 10 times higher in number density at $z = 4$ than at $z = 0$. This relative deficit of group/cluster-sized halos at high-z would be the cause of the clearer break between small and large-scale ACFs at $z = 4$ than $z = 0$. Although multiple occupation of LBGs explains very consistently both the angular scale of transition and the amplitude of large-scale bias, there remains the possibility that the small-scale excess is enhanced or produced by brightening of pair galaxies due to interactions.

3.2. *Luminosity Dependence of Clustering*

We calculate $\omega(\theta)$ and b for six subsamples with limiting magnitudes of $i' < 24.5$, 25.0, 25.5, 26.0, 26.5, and 27.0 (Figure 3). We define the large- and small-scale biases as the biases in the range $40'' < \theta < 400''$ ($1-10h_{100}^{-1}$ Mpc) and $2'' < \theta < 3''$ ($0.05-0.07h_{100}^{-1}$ Mpc), respectively, and show the biases in Figure 4. Although the angular range for the small-scale bias is somewhat arbitrary, the range defined here is beyond the internal structures of galaxies and below the radii of dark halos with $10^{11}M_\odot$, and thus is sensitive to a multiplicity of LBGs in a halo. Luminosity segregation of large-scale clustering is reported for $z = 4$ LBGs (Ouchi et al. 2004b; Allen et al. 2005; Lee et al. 2005). In Figures 3 and 4, we find that ACFs and biases monotonically decrease from $i' < 24.5$ to 27.5 on small scale as well as large scale. Interestingly, Figure 4 shows that the small-scale bias has a stronger dependence on luminosity ($b \simeq 10-50$) than the large-scale bias ($b \simeq 3-4$), and the bottom panels of Figure

3 indicate that outskirts of small-scale excess extend to $\theta \sim 10''$ for bright ($i' < 24.5 - 25.5$) LBGs. All the features of luminosity dependence suggest that bright LBGs reside in more massive dark halos, since massive dark halos have not only a high large-scale bias, but also a high small-scale bias (i.e. high probability of pair galaxies in a massive halo) and an extended outskirt of bias due to a large halo size.

Although the ACFs depart from a power law, we approximate the ACFs with a power law, in order to compare our results with previous results. We fit the ACF over $2-1000''$ with $\omega(\theta) = A_\omega(\theta^{-\beta} - IC/A_\omega)$, where IC is the integral constraint (Groth & Peebles 1977). The bottom panel of Figure 4 presents the best-fit slopes, β, as a function of magnitude. The slopes, β, become flatter at faint magnitudes (see also Kashikawa et al. 2005). This luminosity dependence of β is explained by the strong luminosity dependence of small-scale clustering as discussed above. Then we calculate the Limber equation with the redshift distribution function of Ouchi et al. (2004b), and estimate the correlation lengths, r_0, of spatial two-point correlation function, $\xi = (r/r_0)^{-\gamma}$, where $\gamma = \beta + 1$. Table 1 presents the best-fit parameters, A_ω and β, together with r_0. These r_0 are consistent with those obtained by Ouchi et al. (2004b) as well as by Hildebrandt et al. (2004) and Kashikawa et al. (2005). However, our results are not consistent with those of small-sky surveys in HDF, if we assume that ACF does not significantly evolve between $z = 3$ and 4. For examples, Giavalisco & Dickinson (2001) find a small correlation length of $r_0 = 1.0^{+0.8}_{-0.7} h^{-1}_{100}$ Mpc for $z = 3$ LBGs, while we find a larger value, $r_0 = 3.8^{+0.2}_{-0.2} h^{-1}_{100}$ Mpc, for our $i' < 27.5$ LBGs whose number density is comparable to that of Giavalisco & Dickinson (2001). We restrict our power-law fitting to the same narrow range as Giavalisco & Dickinson (2001) ($1'' \lesssim \theta \lesssim 20''$), and then we obtain the consistent results within errors, i.e. $r_0 = 1.3 \pm 0.3 h^{-1}_{100}$ Mpc and $\beta = 1.9 \pm 0.2$, due to the fitting only to the small-scale excess of the ACF (see Kravtsov et al. 2004). Similarly, the correlation length of red galaxies in HDF-S ($r_0 = 8 h^{-1}_{100}$ Mpc; Daddi et al. 2003) is probably overestimated by the extrapolation from a bump of small-scale ACF with a relatively flat slope of $\beta = 0.8$, which is also claimed by the model of Zheng (2004).

[9] Note that bootstrap errors of the ACF are assumed to be independent.

3.3. *Comparison with a Halo Model*

We fit the halo model of Hamana et al. (2004) to the observed $\omega(\theta)$ and number density, n, simultaneously. This model predicts the $\omega(\theta)$ and n of galaxies contributed by a combination of the 1-halo and 2-halo terms in the framework of the CDM model. The best-fit models are shown in Figure 3 and Table 1. These models account for the overall shape of our ACFs, i.e., the small-scale excess as well as the large-scale clustering (see also Lee et al. 2005), although there remain large residuals [9] (e.g. $\chi^2/\mathrm{dof} = 3.0$ for $i' < 27.5$ LBGs). Reducing these residuals results in a decrease in the combined likelihood ($\omega(\theta) + n$) from the best-fit value. The large residuals imply that we need a more precise model for our LBGs. For implications of the model fitting, Table 1 summarizes the average number of LBGs in a halo, $\langle N_g \rangle$, and the average masses of the halo, $\langle M_h \rangle$, (Hamana et al. 2004) for the best-fit models. The average mass of hosting halos monotonically decreases from $2 \times 10^{12} h^{-1}_{70} M_\odot$ ($i' < 24.5$) to $6 \times 10^{11} h^{-1}_{70} M_\odot$ ($i' < 27.5$). The average number of LBGs in a halo is less than unity, $\langle N_g \rangle \simeq 0.2 - 0.7$, while the model ACF in Figure 3 shows a significant 1-halo term produced by multiple LBGs in one halo. This implies that majority of halos with an average mass have no LBG and only some halos host one or multiple LBG(s).

We thank M. Fall, M. Giavalisco, K. Lee, S. Okamura, and Z. Zheng for helpful comments and discussion.

REFERENCES

Adelberger, K. L., Steidel, C. C., Shapley, A. E., & Pettini, M. 2003, ApJ, 584, 45
Allen, P. D., Moustakas, L. A., Dalton, G., MacDonald, E., Blake, C., Clewley, L., Heymans, C., & Wegner, G. 2005, MNRAS, 523
Arnouts, S., et al. 2002, MNRAS, 329, 355
Bullock, J. S., Wechsler, R. H., & Somerville, R. S. 2002, MNRAS, 329, 246
Benson, A. J., Frenk, C. S., Baugh, C. M., Cole, S., & Lacey, C. G. 2001, MNRAS, 327, 1041
Berlind, A. A., et al. 2003, ApJ, 593, 1
Bertin, E. & Arnouts, S. 1996, A&AS, 117, 393 al. 2002, ApJ, 579, 42
Daddi, E., et al. 2003, ApJ, 588, 50
Foucaud, S., McCracken, H. J., Le Fèvre, O., Arnouts, S., Brodwin, M., Lilly, S. J., Crampton, D., & Mellier, Y. 2003, A&A, 409, 835
Giavalisco, M. & Dickinson, M. 2001, ApJ, 550, 177
Giavalisco, M. 2005, "Wide-Field Imaging from Space", Eds. T. McKay, A. Fruchter, and E. Linder. Elsevier, in press
Groth, E. J. & Peebles, P. J. E. 1977, ApJ, 217, 385
Hamana, T., Ouchi, M., Shimasaku, K., Kayo, I., & Suto, Y. 2004, MNRAS, 347, 813
Hawkins, E., et al. 2003, MNRAS, 346, 78
Hildebrandt, H., et al. 2004, ArXiv Astrophysics e-prints, arXiv:astro-ph/0412375
Kashikawa, N. et al. 2005, submitted to ApJ
Kravtsov, A. V., Berlind, A. A., Wechsler, R. H., Klypin, A. A., Gottlöber, S., Allgood, B., & Primack, J. R. 2004, ApJ, 609, 35
Landy, S. D., & Szalay, A. S. 1993, ApJ, 412, 64
Lee, K. et al. 2005, submitted to ApJ
Ling, E. N., Barrow, J. D., & Frenk, C. S. 1986, MNRAS, 223, 21P
Magliocchetti, M., & Porciani, C. 2003, MNRAS, 346, 186
Mo, H. J. & White, S. D. M. 2002, MNRAS, 336, 112
Moustakas, L. A., & Somerville, R. S. 2002, ApJ, 577, 1 2002, MNRAS, 332, 827
Ouchi, M. et al. 2001, ApJ, 558, L83
Ouchi, M. et al. 2003, ApJ, 582, 60
Ouchi, M., et al. 2004a, ApJ, 611, 660
Ouchi, M., et al. 2004b, ApJ, 611, 685
Ouchi, M., et al. 2005, ApJ, 620, L1
Peacock, J. A., & Dodds, S. J. 1996, MNRAS, 280, L19
Porciani, C., & Giavalisco, M. 2002, ApJ, 565, 24
Sekiguchi, K. et al. 2004, Astrophysics and Space Science Library, 301, 169
Sheth, R. K. & Tormen, G. 1999, MNRAS, 308, 119
Shimasaku, K., et al. 2004, ApJ, 605, L93
van den Bosch, F. C., Yang, X., & Mo, H. J. 2003, MNRAS, 340, 771
Yoshida, M. 2005, Master Thesis, University of Tokyo
Zehavi, I., et al. 2004, ApJ, 608, 16
Zheng, Z. 2004, ApJ, 610, 61

TABLE 1
Summary of Clustering Properties

			Conventional Power-Law Approx.				Model[e]	
$i'_{\rm AB}$ (mag)	$N(<i')$[a]	$n(<i')$[b] (h_{70}^3 Mpc^{-3})	A_ω[c] (arcsec$^\beta$)	β[c]	r_0[c] (h_{100}^{-1} Mpc)	$\beta_{\rm L}$[d]	$\langle Ng\rangle$	$\log\langle M_{\rm h}\rangle$ (h_{70}^{-1} $M_\odot$)
24.5	239	$9.8\pm1.6\times10^{-5}$	10.5 ± 8.2	1.1 ± 0.4	$4.9^{+4.3}_{-4.1}$	$\simeq1.6$	$0.2^{+0.2}_{-0.2}$	$12.3^{+0.1}_{-0.6}$
25.0	808	$2.8\pm0.3\times10^{-4}$	5.0 ± 9.1	0.9 ± 0.3	$5.5^{+1.7}_{-2.1}$	0.9 ± 0.6	$0.3^{+0.4}_{-0.3}$	$12.3^{+0.1}_{-0.2}$
25.5	2231	$6.4\pm0.6\times10^{-4}$	3.1 ± 1.6	0.8 ± 0.1	$5.0^{+0.7}_{-0.8}$	0.8 ± 0.4	$0.6^{+0.1}_{-0.5}$	$12.1^{+0.1}_{-0.1}$
26.0	4891	$1.3\pm0.1\times10^{-3}$	2.6 ± 0.6	0.8 ± 0.1	$5.0^{+0.4}_{-0.4}$	1.0 ± 0.2	$0.6^{+0.1}_{-0.1}$	$12.0^{+0.1}_{-0.1}$
26.5	8639	$2.2\pm0.3\times10^{-3}$	0.6 ± 0.1	0.5 ± 0.1	$4.8^{+0.2}_{-0.3}$	0.7 ± 0.2	$0.6^{+0.1}_{-0.1}$	$11.9^{+0.05}_{-0.05}$
27.0	12921	$3.7\pm0.7\times10^{-3}$	0.8 ± 0.1	0.6 ± 0.1	$4.4^{+0.1}_{-0.2}$	0.7 ± 0.1	$0.6^{+0.1}_{-0.2}$	$11.8^{+0.07}_{-0.04}$
27.5	16920	$5.8\pm1.4\times10^{-3}$	0.5 ± 0.1	0.5 ± 0.1	$3.8^{+0.2}_{-0.2}$	0.6 ± 0.1	$0.7^{+0.2}_{-0.1}$	$11.8^{+0.02}_{-0.05}$

[a]Cumulative numbers. Differential surface densities are 0.002 ± 0.001, 0.014 ± 0.002, 0.049 ± 0.004, 0.158 ± 0.007, 0.395 ± 0.011, 0.739 ± 0.014, 1.041 ± 0.017, 1.189 ± 0.018, and 1.111 ± 0.018 arcmin^{-2} (0.5mag)$^{-1}$ for $i'=23.25$, 23.75, 24.25, 24.75, 25.25, 25.75, 26.25, 26.75, and 27.25, respectively, which are consistent with previous measurements (e.g. Ouchi et al. 2004a).

[b]Cumulative number density calculated from luminosity function of Giavalisco (2005).

[c]Results from the conventional power-law approximation, i.e. $\omega(\theta)=A_\omega(\theta^{-\beta}-IC/A_\omega)$, over $2''-1000''$. For integral constraints, IC, we apply $IC/A_\omega=[3,14,21,28,364,154,293]\times10^{-4}$ for $i'=[24.5,25.0,25.5,26.0,26.5,27.0,27.5]$.

[d]Power-law slope for the fit of $\omega=A_{\omega{\rm L}}\theta^{-\beta_{\rm L}}$ over $40''-400''$ with no IC correction.

[e] χ^2/dof $=[0.7,0.4,2.5,6.9,8.3,7.1,3.0]$ for $i'=[24.5,25.0,25.5,26.0,26.5,27.0,27.5]$.